Nipah virus Malaysia and Bangladesh strain-induced pathogenesis in mice lacking type I interferon receptor signaling

Short title: Comparative pathogenesis of Nipah virus strains in IFNAR KO mice

Authors

Lucia Amurri[1], Olivier Reynard[1], Ilona Ronco[1], Daniel Déri[3,4], Bernadett Pályi[3,4], Julia Spanier[2], Jennifer Skerra[2], Olivia Terceve[6], Thibaut Larcher[6], Ulrich Kalinke[2,7], Zoltán Kis[3,4,5], Branka Horvat[1], Mathieu Iampietro[1*]

Affiliations

[1] CIRI, Centre International de Recherche en Infectiologie, INSERM U1111, CNRS, UMR5308, Univ Lyon, Université Claude Bernard Lyon 1, École Normale Supérieure de Lyon, 21 Avenue Tony Garnier, 69007 Lyon, France.

[2] Institute for Experimental Infection Research, TWINCORE, Centre for Experimental and Clinical Infection research, a joint venture between the Helmholtz-Centre for Infection Research and the Hannover Medical School, Hannover, Germany.

[3] National Biosafety Laboratory, National Center for Public Health and Pharmacy, Budapest, Hungary.

[4] Semmelweis University, Institute of Medical Microbiology, Budapest, Hungary.

[5] European Research Infrastructure on Highly Pathogenic Agents (ERINHA-AISBL), Brussels, Belgium.

[6] UMR703, PAnTher, APEX, Oniris VetAgroBio, La Chantrerie, CS 40706, 44307 Nantes, France

[7] Cluster of Excellence - Resolving Infection Susceptibility (RESIST, Hannover Medical School, EXC 2155), Hannover, Germany.

* Corresponding author

E-mail: mathieu.iampietro@inserm.fr

Abstract

Nipah virus (NiV) is a zoonotic highly pathogenic *Paramyxovirus* inducing lethal outbreaks of encephalitis and severe acute respiratory syndrome (SARS) with an average case-fatality rate of 75%. Two viral strains, NiV-Malaysia (NiV-Mal) and NiV-Bangladesh (NiV-Ban), associated to distinct geographical distribution, route of transmission, symptoms and lethality have been described. Due to the permanent threat of these emerging infections and the lack of approved therapeutics, it is crucial to improve our understanding regarding NiV-associated pathogenesis. Mice represent a small and accessible animal model, provided with numerous biological tools for the functional assessment of different genes related to antiviral response. Here, we analyze the susceptibility of mice deficient for type I interferon receptor (IFNAR KO) to infection with either NiV-Mal or NiV-Ban through intraperitoneal or intranasal routes. Our results show that IFNAR KO mice are susceptible to NiV-Ban infection via intraperitoneal route, although to a lesser extent than NiV-Mal, and develop encephalitis and pulmonary syndrome with viral propagation to different organs and lethal outcome in 60% of infected animals. In addition, intranasal administration of both viral strains led to a subclinical infection with viral replication in brain and lungs and production of virus-specific neutralizing antibodies. These results indicate IFNAR KO mice as a small animal model permitting comparative studies of the immunopathogenesis perpetrated by both NiV-Mal and NiV-Ban infections.

Author summary

Availability of small animal models represents a major issue to characterize virus-associated pathogenesis to further implement therapeutic strategies. Previous studies performed with NiV-Mal and NiV-Ban strains in wild-type (WT) mice did not indicate signs of NiV disease. However, when challenged with NiV-Mal, IFNAR KO mice suffered fatal outcomes, thus providing useful information on viral immunopathogenesis. Surprisingly, while being the more frequently re-emerging virus strain, no infection studies with NiV-Ban have been performed in IFNAR KO mice so far. Here, we sought comparing pathogenesis after NiV-Mal- and NiV-Ban-infection following IP and IN inoculations in IFNAR KO mice. Indeed, our results highlighted that contrary to fatal IP challenge, IN inoculation lead to a subclinical infection with both NiV strains. Moreover, we determined that NiV-Mal is more pathogenic than NiV-Ban following IP infection. Finally, distinct histopathological manifestations and tropism were associated with each viral strain and specific route of infection. Overall, our study implies that IFNAR KO mice represent a useful animal model to study strain-specific NiV pathophysiology.

Introduction

Nipah virus (NiV) is an emerging zoonotic *Paramyxovirus* causing highly lethal outbreaks in South-East Asia, Bangladesh and India (1). NiV is naturally hosted by *Pteropus* fruit bats, which are widespread in tropical and subtropical areas of Asia and Indian/Pacific Ocean islands and Australia (2,3). Due to its high pathogenicity, its human-to-human transmission and the lack of approved treatments or vaccines, World Health Organization has included NiV in the Blueprint list of epidemic threats requiring urgent research and development actions (4). Moreover, climate change, deforestation and intensive farming are progressively disrupting the habitats of reservoir animals and increasing animal-human contacts, leading to an increased risk for epidemic or pandemic (5–9).

Two NiV strains have been described, NiV Malaysia (NiV-Mal) and NiV Bangladesh (NiV-Ban), that share 91.8% of nucleotide sequence homology but show remarkable differences in epidemiology and human pathology (8,10). The first NiV outbreak was registered in Malaysia in 1998-1999, where the virus was first transmitted from asymptomatic fruit bats to pigs as intermediate hosts before infecting humans (11). This led to 265 cases of acute encephalitis and 105 deaths (case fatality rate, CFR=40%), mostly among pig farmers who were exposed to infected animals.

A second NiV strain emerged in Bangladesh in 2001 through a direct spillover from bats to humans following the consumption of contaminated date palm sap (12). Indeed, in this geographical area sap is harvested from palm trees using reservoirs where bats can approach and contaminate the juice with saliva and/or urine (13). Moreover, in addition to animal-to-human transmission, respiratory human-to-human transmission has been reported (14). While NiV-Mal is commonly associated with lethal encephalitis, NiV-Ban patients mainly display severe respiratory syndrome in addition to neurological symptoms. Since 2001, NiV-Ban is re-emerging frequently in Bangladesh and India, with an average CFR around 75%, reaching up to 100% in some outbreaks and presenting constant threat for new episodes and possible pandemic spread (15–17).

NiV can infect a wide range of mammals by interacting with the highly-conserved and ubiquitously expressed Ephrin B2 and B3 receptors (18–20). However, while humans, pigs and different animal models such as non-human primates (NHP), hamsters and ferrets, develop clinical symptoms with high lethality following NiV infection, mice clear the virus despite being permissive to infection (21–23). To efficiently and better characterize viral pathogenesis, convenient animal models are needed. Indeed, while several studies using the hamster model have allowed the establishment a pre-clinical approach including both NiV strains and both intraperitoneal (IP) and intranasal (IN) route of infections (24), the development of an appropriate mouse model would represent an important progress to further decipher NiV pathogenesis *in vivo*.

In previous studies using NiV-Mal infection in both wild type (WT) and Interferon α/β receptor knock out (IFNAR KO) mice, all WT animals survive both IP and IN challenge while 100% and 60% of IFNAR KO mice succumb to NiV-Mal challenge, respectively (23,25–27). In addition, viral dissemination in the brain, lungs, spleen and liver, along brain-associated lesions, leading to neurological symptoms, were observed in IP-inoculated IFNAR KO mice (25). Afterwards,

101 additional works have been conducted on NiV infection in WT mice (28,29), notably Dups *et al.*
102 compared NiV-Mal and NiV-Ban infections in intranasally infected WT mice (28). All animals
103 survived without developing disease, and both viral RNA and viral antigens were detected in the
104 lungs of infected animals only, suggesting that WT mice were able to control viral dissemination,
105 with no significant differences between both viral strains. Moreover, neutralizing antibodies (nAb)
106 response was not detected. These observations were recently confirmed by Edwards *et al.*, who
107 analyzed NiV-Ban IN infection in WT mice where all animals survived without displaying neither
108 clinical symptoms nor histological lesions, with viral detection only in the lungs and a mild
109 production of nAb in 3 out of 5 mice (29).

110 Importantly, contrary to NiV-Mal, NiV-Ban infection has not been evaluated in IFNAR KO mice
111 yet. Here, we compare pathogenesis in both WT and IFNAR KO mice infected with NiV-Mal or
112 NiV-Ban through IP or IN route.

113 First, we demonstrated the permissiveness of primary murine embryonic fibroblasts (MEFs)
114 derived from WT and IFNAR KO mice to both NiV strains *in vitro*. Then, we analyzed the
115 susceptibility of both mouse genotypes to NiV-Mal or NiV-Ban following IP or IN infection *in*
116 *vivo*. We observed that NiV-Mal was more virulent than NiV-Ban in IP-infected IFNAR KO mice.
117 Surprisingly, neither NiV-Mal nor NiV-Ban lead to fatal outcome following IN infection in
118 IFNAR KO mice. Moreover, viral genome quantification and histopathological analysis were
119 performed on harvested organs to determine the magnitude of viral spread and tropism. While IN
120 virus inoculation was associated to a subclinical infection in all experimental groups, IP infection
121 exerted significantly higher viral replication and tissular pathology in IFNAR KO compared to
122 WT mice. Interestingly, both viral strains presented different cellular tropism and syncytia
123 distribution in the lungs of IFNAR KO animals.

124 Globally, these results suggest that IFNAR KO mice can be used as a small animal model for
125 fundamental and pathophysiology studies of both NiV-Mal and NiV-Ban infections, taking
126 advantage of numerous biological tools available for murine studies.

127 # Materials and methods

128 ## Ethical statement

129 Animal experiments were performed in the biosafety level 4 (BSL-4) facility of the National
130 Biosafety Laboratory in Budapest according to the guidelines of the European Communities
131 Council Directive (86/609 EEC) and were approved by the Hungarian National Authority
132 (Scientific Ethics Council for Animal Experiments, PE/EA/1456-7/2020).

133 ## Mice

134 Wild type (WT) C57BL/6J mice (Charles River) and B6.129S2-Ifnar1tm1(Neo)Agt (IFNAR-KO)
135 mice (30) were bred under specific pathogen-free conditions in the central mouse facility of the
136 Helmholtz Centre for Infection Research (Brunswick), at TWINCORE (Centre for Experimental
137 and Clinical Infection Research, Hanover, Germany) and at Plateau de Biologie experimentale de
138 la souris (PBES) in Lyon. Mouse experimental work was carried out using 3-week-old to 6-week-
139 old mice with equal male-female distribution. Mice were kept under BSL-4 conditions in
140 individually ventilated cages (IsoRat ISO48NFEEU, Techniplast, Italy), housed on autoclaved
141 corn bedding (Rehofix, J. Rettenmaier & Söhne GmbH + CO KG, Rosenberg, Germany), fed
142 autoclaved food (VRFI (P), Special Diet Services) ad libitum, given osmosis-treated water
143 provided in bottles ad libitum, and the cages were equipped for proper environmental enrichment.

144 ## Cell lines

145 WT or IFNAR KO primary murine embryonic fibroblasts (MEFs) were isolated from murine
146 embryos obtained from female pregnant mice 13 days after conception (26,31) and cultured in
147 Dulbecco's modified Eagle's medium (DMEM) GlutaMAX supplemented with 10% heat-
148 inactivated fetal bovine serum (FBS), 0.2% 2-mercaptoethanol, 1% HEPES, 1% nonessential
149 amino acids, 1% sodium pyruvate, and 2% penicillin-streptomycin mix at 37°C with 5% CO2.

150 WT and IFNAR KO MEFs were plated in 12-well plates ($1.5x10^5$ cells/well) or in 24-well plates
151 ($5x10^4$ cells/well) for immunofluorescence or RT-qPCR analysis, respectively. MEFs were then
152 infected in the Jean Mérieux BSL-4 facility in Lyon with NiV-Mal or NiV-Ban at a multiplicity
153 of infection (MOI) of 0.3 plaque-forming units (PFU)/cell (according to the viral titer previously
154 calculated on Vero E6 cells) for 1h at 37°C in DMEM 0% FBS. Then, virus-containing medium
155 was removed and substituted with fresh complete medium before being incubated for 24h or 48h
156 at 37°C.

157 ## Viruses

158 NiV-Mal (isolate UMMC1 GenBank- AY029767) and NiV-Ban isolate SPB200401066 (GenBank
159 AY988601, kindly provided by the Center for Disease Control and Prevention, Atlanta USA) were
160 prepared by infecting Vero E6 cells (ATCC CRL-1586TM) cultured in DMEM, in the INSERM
161 Jean Mérieux BSL-4 in Lyon, France.

162 ## Intraperitoneal and intranasal infection of mice

163 All work involving live NiV-Mal and NiV-Ban infectionswas performed under BSL-4 conditions.
164 All mice were inoculated intraperitoneally with 10^6 PFU of NIV-Mal or NiV-Ban or intranasally
165 with 10^5 PFU of NiV-Mal or NiV-Ban under inhalational anesthesia with isoflurane (isoflurane:
166 ISOFLUTEK 1000 mg/g, Laboratorios Karizoo S.A.; anesthesia station: MiniHUB-V3, TEM
167 SEGA, France).

168 Following infection, animals were weighed and monitored on a daily basis as part of a scoring
169 system to follow the symptoms and determine endpoint euthanasia. After NiV-Mal infection,
170 animals were monitored for 32 days and organs were collected at the end of the experiment or at
171 the day of death. For NiV-Ban infection, animals were monitored during 1-month post-infection,
172 and in addition programmed euthanasia was performed for 4 hours, 1 day, 2 days, 4 days, 7 days
173 or 10 days post-infection (d0+4h, d1, d2, d4, d7, d10), and at the end of the protocol in case of
174 mice which survived infection. For graphical representations of qPCR data and statistical analyses,
175 murine samples were pooled and grouped into early (from d0+4h to d1), mid (from d2 to d7) and
176 late (after d7 until d32) phase of infection.

177 Sample collection and preparation

178 Euthanasia with CO_2 was conducted under inhalational anesthesia with isoflurane, followed by
179 blood collection via cardiac puncture and autopsy. During autopsy, brains, lungs, spleens and livers
180 were collected for further nucleic acid isolation and histological analysis. Organs were divided for
181 molecular testing and were collected and frozen immediately at -80°C without any medium until
182 further preparation. Parts of organs for immunohistochemistry were collected into fixative 10
183 V/V% formaldehyde-PBS solution. Then, 25-30 mg of the thawed organs were taken into MagNA
184 Lyser Green Beads tubes (Roche Diagnostics GmbH, Mannheim, Germany) containing 600 µL of
185 1:100 mixture of β-mercaptoethanol and Buffer RLT (QIAGEN GmbH, Hilden, Germany). After
186 homogenization using MagNA Lyser instrument (Roche Diagnostics GmbH), samples were
187 centrifuged for 5 minutes at 12000 rpm. Supernatants were transferred into new tubes and after 10
188 min of incubation at room-temperature, an equal volume of 70 V/V% ethanol was added into each
189 tube.

190 Seroneutralization

191 Seroneutralization assay was performed on mice euthanized after day 7. Serum samples were
192 stored at -80°C without previous thawing and were analyzed without heat inactivation. Serum
193 dilution and assay procedures were done according to manufacturer's instructions under BSL-4
194 conditions. Sera were diluted in 7-point serial two-fold dilutions in triplicate in serum-free DMEM
195 in sterile 96-well microtiter plates. Positive and negative control sera were also applied, the latter
196 with and without serum as well. Equal volume of 60±20 TCID50 NiV-Mal or NiV-Ban was added
197 into each well and incubated for 1 h at 37°C. Then, samples were transferred on a Vero E6 cells
198 monolayer (approximately $1{,}8 \times 10^5$ cells/mL) maintained in serum-free DMEM in 96-well plates
199 (TPP, Switzerland). The neutralizing antibody titer of each sample was determined by the lack of
200 cytopathic effect (CPE) after a 5 days incubation at 37°C. For triplicates the geometric mean of
201 end dilutions was calculated and reported as a neutralizing antibody titer (nAb).

202 ## RNA extraction and RT-qPCR

203 For murine samples, total nucleic acid extraction was performed using QIAsymphony SP
204 instrument with QIAsymphony DSP Virus/Pathogen Mini Kit and Complex200_OBL_V4_DSP
205 protocol (QIAGEN GmbH, Hilden, Germany). Quality control of samples qPCR was performed
206 targeting the Peptidylprolyl Isomerase A (Ppia) housekeeping gene of the mouse as previously
207 described (32). The reaction was performed on LightCycler 480 Platform II using LightCycler®
208 Multiplex RNA Virus Master kit (Roche Lifesciences), and data were analyzed with LightCycler®
209 480 SW 1.5.1 software using Abs Quant/2nd Derivative Max method.

210 For *in vitro* MEF experiments, cells were collected at indicated time points and RNA was extracted
211 using NucleoSpin RNA Kit (Macherey Nagel) or QIAamp Viral RNA mini-Kit (Qiagen) on cells
212 and supernatants, respectively, according to manufacturer's instructions.

213 Extracted RNA was amplified by real-time (RT) quantitative (q) PCR using Luna Universal One-
214 Step RT-qPCR Kit (NEB) on a StepOnePlus Real-Time PCR System. Pfaffl Model (33) and Bustin
215 MIQE checklist (34) were used for all validations and calculations. To validate our primers, a PCR
216 on a positive control has been performed before dosing 10^{-1} to 10^{-12} 10-fold dilutions of our PCR
217 products using the Denovix DS-11-FX spectrophotometer to evaluate the quantity of DNA in each
218 dilution. Then, the serial dilutions were run in qPCR to validate efficacy, specificity and sensitivity
219 of each couple of primers. Moreover, the exact number of copies in each qPCR reaction was
220 obtained by calculating the "N0 Samples = N0 Standard $*$ Efficacy-ΔCt" before being converted
221 using molecular weight of each targeted gene and Avogadro number. Results obtained were
222 converted to "copies/µg of RNA" for cell lysate samples. Finally, normalization was performed
223 by dividing obtained numbers of RNA copies of the target genes with the deviation of the mouse
224 glyceraldehyde 3-phosphate dehydrogenase (mGAPDH) used as housekeeping gene. Specific set
225 of primers were designed and validated for the detection of mGAPDH (forward:
226 GCATGGCCTTCCGTGTCC; reverse: TGTCATCATACTTGGCAGGTTTCT) and viral NiV-N
227 (forward: GGCAGGATTCTTCGCAACCATC, reverse: GGCTCTTGGGCCAATTTCTCTG).

228 ## Immunofluorescence

229 MEFs cultured in 12-well plates were washed with PBS 1X and fixed with PFA 4% for 20 min at
230 4°C. After 2 washes with PBS 1X, cells were permeabilized with TritonX100 0.1%-PBS for 10
231 min and blocked with of bovine serum albumin (BSA) 2.5%-PBS for 10 min. After 2 washes with
232 PBS-2% FCS-0.1% Tween, cells were incubated 1h at room temperature (RT) with an in-house
233 produced rabbit anti-NiV nucleoprotein (NiV-N) I Ab 1/300 in PBS-2% FCS-0.1% Tween. Plates
234 were then washed 2 times with PBS-2% FCS-0.1% Tween, incubated 1 h at room temperature
235 with a mix of fluorophore-conjugated secondary antibody (anti-mouse AF488, Invitrogen) and
236 DAPI (Merck) 1:1000. Finally, slides were washed 2 times with PBS-2% FCS-0.1% Tween, once
237 with PBS 1X, covered in PBS 1X and stored at 4°C. Fluorescence was evaluated using a Zeiss
238 Axio OBSERVER Z.1 microscope, and photographs were treated using ImageJ software version
239 Java 1.8.0_112.

240 ## Histology and immunohistochemistry

241 For histopathological evaluation, formalin-fixed specimens were embedded in paraffin wax, 4 µm
242 tissue sections were processed and stained with hematoxylin-eosin-saffron (HES).
243 Immunohistochemistry was performed using the Ventana Discovery Ultra Instrument (Ventana
244 Medical Systems, Roche Diagnostics). The sections were dewaxed and rehydrated. Slides were
245 pre-treated with CC1 (pH 8, Roche Diagnostics) at 98 °C for 40 min. They were then incubated
246 for 30 min at room temperature with blocking buffer (Diagomics), followed by a 1-hour incubation
247 at 37 °C with the primary antibody, rabbit polyclonal anti-NiV-N (1:250). After rinsing, slides
248 were incubated for 30 min at room temperature with a biotinylated goat anti-rabbit IgG antibody
249 (1:200, Dako). Immunoreactive complexes were visualized using streptavidin-conjugated
250 horseradish peroxidase (1:200, Dako) and DAB chromogen (Fisher Scientific). Sections were
251 counterstained with Hematoxylin II and examined using a Nikon Eclipse Ni microscope equipped
252 with a Nikon DS-Ri color camera. Histopathological analysis was performed by a board-certified
253 veterinary pathologist.

254

255 # Results

256 **NiV-Mal replicates at higher levels compared to NiV-Ban in IFNAR KO primary murine**
257 **cells**

258 The replication and cytopathic effects of NiV-Mal and NiV-Ban were initially analyzed *in vitro* in
259 primary mouse embryonic fibroblasts (MEFs) obtained from WT and IFNAR KO mice sharing
260 the same genetical background employed in further *in vivo* study. Both MEFs genotypes were
261 infected with either NiV strains (MOI = 0.3) and then cell lysates along supernatants were collected
262 at 0h immediately after viral inoculation and at 24h and 48h post infection (Fig.1). NiV-N protein
263 and mRNA levels were analyzed through immunofluorescence (Fig. 1A-1D) and RT-qPCR (Fig.
264 1E and 1F), respectively. Both cell types were permissive to both NiV strains, although NiV-Ban
265 showed a reduced replication compared to NiV-Mal (Fig. 1A-1F). Also, both viral strains
266 replicated at higher levels in IFNAR KO cells compared to WT cells (Fig. 1A-1D). Moreover,
267 multiple NiV-Mal-induced syncytia appeared 24h post infection and progressively expanded until
268 48h post infection (Fig. 1A and 1C). Conversely, syncytial multi-nucleated cells were observed
269 only at 48h following NiV-Ban infection (Fig. 1B and 1D) associated with a lower replication rate
270 compared to NiV-Mal infected-cells (Figure 1E and 1F). Globally, NiV-Mal replicated faster than
271 NiV-Ban, resulting in higher levels of viral genomes both produced in the cells and released in the
272 supernatant (Fig. 1A-1F).

273

274 **Fig. 1. NiV-Mal expands at faster rate than NiV-Ban in primary murine cells.** Murine embryonic
275 fibroblasts (MEF) derived from WT or IFNAR KO mice where mock-infected (NI) or infected with NiV-
276 Mal or NiV-Ban at a MOI of 0.3 and cells were cultured for 0h, 24h or 48h (n=3). (A-D) Cells were fixed
277 and stained with DAPI and anti-NiV nucleoprotein (NiV-N) antibody and evaluated by fluorescence
278 microscopy. (E-F) NiV-N mRNA levels from MEF cell lysates and supernatants were assessed by real time
279 RT-qPCR. Data are represented as mean ± standard deviation (SD) of three independent replicates. The
280 difference between NiV-Mal and NiV-Ban in IFNAR KO mice was analyzed using two-way analysis of
281 variance, followed by a Tukey multiple comparison test: ns (not significant); ****$p<0.0001$.

282

283 **NiV-Mal infection is more severe than NiV-Ban following challenge in IFNAR KO mice**

284 We next compared NiV-Mal and NiV-Ban infection in murine models *in vivo.* We infected WT
285 and IFNAR KO mice through IP or IN route with 10^6 and 10^5 PFU of virus, respectively of the
286 route of infection, and monitored the animals for 32 days (Fig. 2 and S1).

287 While all WT mice survived IP infections, all NiV-Mal IP-infected IFNAR KO mice succumbed
288 at a mean day of death 6 ± 1.4 days, while NiV-Ban IP infection provoked the death of 60% of
289 mice with a mean day of death of 9.6 ± 2.9 (Fig. 2A). NiV-Mal- and NiV-Ban-infected mice which
290 succumbed to the infection showed similar symptoms, including loss of weight, ruffled hair, facial
291 pain and paralysis (Fig. S1A-S1D). Moreover, 3 IFNAR KO mice IP-infected with NiV-Mal that
292 died at day 5 or day 6 displayed breathing difficulties (Fig. S1C). In contrast, all IN-infected
293 IFNAR KO mice survived until the end of the experiment (Fig. 2B). Intriguingly, one IN-infected

294 WT mouse out of five succumbed NiV-Mal infection and was found dead at d20 (Fig. 2B), despite
295 not showing symptoms throughout the experiment (Fig. S1D). Following IP infection, all WT mice
296 produced specific anti-NiV neutralizing antibodies (nAb) (Fig. 2C). NiV-Mal IP-infected IFNAR
297 KO animals did not produce nAb, consistent with the fact that they all died before day 10, whose
298 period was too short to develop a humoral response (Fig. 2C). Concerning NiV-Ban IP-infected
299 animals, both animals surviving viral challenge produced nAb, thus confirming their initial
300 infection (Fig. 2C). Finally, following IN infection, IFNAR KO mice produced significantly more
301 nAb antibodies than WT mice after infection with either viral strain (Fig. 2D).

302

303 **Fig. 2. NiV-Mal and NiV-Ban perpetrate different pathogenicity in mice *in vivo*.** WT and IFNAR KO
304 mice were infected through an intraperitoneal route (IP) or intranasal route (IN) with 10^6 or 10^5 plaque
305 forming units (PFU), respectively, of NiV-Mal or NiV-Ban. All groups were constituted of 5 animals except
306 for NiV-Mal IFNAR KO group, which consisted of 6 mice. (A-B) Survival of infected mice was followed
307 up for 32 days. Survival was analyzed using Gehan-Breslow-Wilcoxon test. *$p<0.05$. (C-D) Virus-specific
308 neutralizing antibodies (nAb) titer was evaluated by seroneutralization in sera collected at the day of
309 euthanasia (empty dots) or at the end of the experiment (full dots). Serum could not be collected for the
310 NiV-Mal IN-infected mouse which was found dead at d20. Horizontal lines correspond to the average nAb
311 titer of each group. ND = non detected. Data are represented as mean ± standard error mean (SEM). Samples
312 were analyzed using Kruskal Wallis and Dunn's multiple comparison test, *$p<0.05$, **$p<0.01$.

313

314 **NiV-Mal disseminates at higher levels compared to NiV-Ban following intraperitoneal**
315 **infection in IFNAR KO mice**

316 To characterize viral replication and expansion, NiV-N RNA levels were quantified in the brain,
317 lung, spleen and liver of infected animals (Fig. 3). As we have previously analyzed NiV-Mal
318 infection in details (25), in the present only one group of NiV-Mal-infected animals was included
319 and monitored during one month (Fig. 3A-3D, left panels). To characterize early events following
320 infection with NiV-Ban strain which has not been tested in IFNAR KO mice before, two groups
321 of mice were infected with NiV-Ban (Fig. 3A-3D, right panels). The first group was monitored
322 until d32, and in the second one single mice were euthanized at defined time points, ie., +4h, d1,
323 d2, d4, d7, d10). For biological accuracy and consistency with our previous study, RT-qPCR data
324 from the two groups of NiV-Ban-infected mice were pooled and represented as "early" (+4h - d1),
325 "mid" (d2 - d7) and "late" (d8 - d32) periods (Fig. 3A-3D, right panels).

326 Both strains of NiV were detected in the brain (Fig. 3A), lung (Fig. 3B), spleen (Fig. 3C) and liver
327 (Fig. 3D) of IP-infected IFNAR KO mice. No viral RNA was detected in any tested organ of WT
328 animals infected with NiV-Mal analyzed at d32, thus demonstrating effective viral control (Fig.
329 3A-3D, left panels). NiV-Ban IP-infected WT mice showed active viral replication throughout
330 early, mid and late phases, and still almost completely cleared the infection by d32 (Fig. 3A-3D,
331 right panels). Three WT mice were positive for NiV-Ban in the brain in the early phase of infection,
332 however, viral RNA was no longer detected in the brain throughout the following month (Fig. 3A,
333 right panel). Among IFNAR KO brain samples, 6 out of 6 were virus-positive after NiV-Mal
334 infection, while only 5 out of 17 were virus-positive following NiV-Ban infection (Fig. 3A, left

335 panel and 3A, right panel). Interestingly, 4 out of 6 NiV-Ban-infected IFNAR KO mice had high
336 levels of NiV-N RNA in the brain at the late phase of infection (Fig. 3A, right panel). Out of these
337 4 mice, one underwent programmed euthanasia at d10, two succumbed due to infection at d10 and
338 d13, and one survived until d32 without clinical signs. While the animals euthanized at d10 and
339 d13 had viral RNA in lung and spleen as well (Fig. 3B and 3C, right panels), the one that reached
340 d32 did not have NiV-N in any other organs except for the brain (Fig. 3A-3D, right panels).

341

342 **Fig. 3. Intraperitoneal NiV infection favors viral dissemination in IFNAR KO mice.** (A-D) WT (up
343 blue triangle and down red triangle) and IFNAR KO (light blue circle ang light red square) mice were
344 inoculated intraperitoneally with 10^6 PFU of NiV-Mal (A-D, left graphs) or NiV-Ban (A-D, right graphs).
345 Following NiV-Mal infection, NiV nucleoprotein (NiV-N) mRNA levels in murine brains (A, left), lungs
346 (B, left), spleens (C, left) and livers (D, left) were harvested either at d32 from surviving WT mice (full
347 dots) or at the day of death of IFNAR KO mice (empty dots) and were assessed by RT-qPCR. Following
348 NiV-Ban infection, NiV-N mRNA levels in murine brains (A, right), lungs (B, right), spleens (C, right) and
349 livers (D, right) were harvested at the day of death (empty dots) or programmed euthanasia (full dots) and
350 were assessed by RT-qPCR. For graphical representation and statistical analyses, mice samples were pooled
351 into early (from d0+4h to d1), mid (from d2 to d7) and late (until d32) phase of infection. Horizontal lines
352 correspond to the average of each group. The statistical difference between IFNAR KO and WT mice
353 groups was analyzed using Mann Whitney test: ns (not significant); *$p<0.05$; **$p<0.01$.

354

355 **NiV-Mal and NiV-Ban dissemination is limited following intranasal infection in IFNAR KO**
356 **mice**

357 Following IN infection with both NiV strains, most animals were negative for NiV-N mRNA,
358 consistent with the fact that, despite one fatal outcome, all other animals survived without major
359 clinical signs (Fig. 4). In contrast, the only WT mouse that succumbed to NiV-Mal infection at
360 d20 was found positive to NiV-N in both brain and lungs (Fig. 4A and 4B, left panels). Contrary
361 to IP-infected animals, no significant differences were detected between IN-infected WT and
362 IFNAR KO mice (Fig. 4A-4D, left and right panels). The most affected organ resulted to be the
363 lung, where virus was detected in approximately 30% of animals (3/10 NiV-Mal-infected mice
364 and 14/45 NiV-Ban-infected mice) (Fig. 4B, left and right panels). Spleens and livers were all
365 negative to NiV-Mal RNA (Fig. 4C and 4D, left panels) and only two IFNAR KO mice were
366 positive to NiV-Ban at mid/late time points, consistent with the IN route of infection (Fig. 4C and
367 4D, right panels). The brains of two WT and one IFNAR KO animals infected with NiV-Mal were
368 positive for NiV-N RT-qPCR (Fig. 4A, left panel), while the four brain samples that were positive
369 throughout NiV-Ban infection experiment were all collected from IFNAR KO mice (Fig. 4A, right
370 panel).

371

372 **Fig. 4. Intranasal NiV infection is controlled in IFNAR KO mice.** (A-D) WT (up green triangle and
373 down purple triangle) and IFNAR KO (light green circle ang light purple square) mice were inoculated
374 intraperitoneally with 10^5 PFU of NiV-Mal (A-D, left graphs) or NiV-Ban (A-D, right graphs). Following
375 NiV-Mal infection, NiV nucleoprotein (NiV-N) mRNA levels in murine brains (A, left), lungs (B, left),

spleens (C, left) and livers (D, left) were harvested either at the day of death (d20, empty dot) or d32 from surviving WT mice (full dots) and IFNAR KO mice (full dots) and were assessed by RT-qPCR. Following NiV-Ban infection, NiV-N mRNA levels in murine brains (A, right), lungs (B, right), spleens (C, right) and livers (D, right) were harvested at day 32 (full dots) and were assessed by RT-qPCR. For graphical representation and statistical analyses, mice samples were pooled into early (from d0+4h to d1), mid (from d2 to d7) and late (until d32) phase of infection. Horizontal lines correspond to the average of each group. The statistical difference between IFNAR KO and WT mice groups was analyzed using Mann Whitney test: ns (not significant).

Intranasal infection of both NiV-Mal and Niv-Ban induces a milder immunopathogenesis compared to intraperitoneal infection in IFNAR KO mice

To better characterize NiV-Mal and NiV-Ban-related pathology, we performed a histopathological analysis and immunolabeling of NiV-N antigen on selected brain, lung and/or spleen sections (Fig. 5, 6, S2 and S3). We prioritized analysis of samples from IP-infected mice that succumbed or were euthanized between d4 and d13 post-infection, corresponding to the critical period of infection (Fig. 5 and 6). Also, NiV-Mal IP-infected WT mice, that all survived until d32, were added to the analysis as controls (Fig. 5, 6, S2 and S3). Indeed, all WT mice resulted negative to NiV-N labeling following both NiV-Mal and NiV-Ban IP infections and did not display major histological signs (Fig. 5A, left panel and S2). Contrary to WT animals, three IFNAR KO mice which succumbed to NiV-Mal infection between d5 and d6 were positive for the presence of NiV-N protein (Fig. 5A, left panel and 5B). NiV-N labeling was found in the brain, in meningeal vessels and olfactory bulb, respectively, with a characterized infiltration of granulocytes (Fig. 5A, left panel and 5B). In the lung, NiV-N localized in bronchial epithelium, some pneumocytes and mononuclear cells of the Bronchi-Associated Lymphoid Tissue (BALT) (Fig. 5B). The detection of some virus in the lung was associated in all 3 animals with vascular lesions including syncytial cells in the endothelium, vascular wall damage, perivascular inflammation and edema (Fig. 6).

Fig. 5. NiV infection level is higher following intraperitoneal infection compared to intranasal infection in IFNAR KO mice. Organs from selected animals were included in paraffin and sections were stained with a rabbit polyclonal anti-NiV-N antibody and DAPI for immunohistochemistry analysis. (A) A scoring system was applied by a veterinary pathologist (0=no labelling; 1=a few positive cells; 2=small clusters of positive cells; 3=multiple large or extensive foci of positive cells) on slides obtained from IP- (left panel) or IN-infected (right panel) organs, respectively. Empty dots represent animals succumbed or euthanized in early/mid late phases of infection (until day 10). (B) Brain, lung and spleens sections from WT mice were used as NiV-negative control conditions while similar sections from IFNAR KO mice were used to characterize the presence of NiV-N antigens following infection. NS/NA represents samples were NiV-N was not shown/not analyzed. Scale bar represents the size of analyzed portions.

Fig. 6. Intraperitoneal NiV infection generates extended immunopathogenesis compared to intranasal infection in IFNAR KO mice. Organs from selected animals underwent hematoxylin-eosin-saffron (HES) staining and were evaluated by a board-certified veterinary pathologist. Brain, lung and

417 spleens sections from WT mice were used as control conditions while similar sections from IFNAR KO
418 mice were used to characterize the presence of immunopathogenic manifestations following NiV infection.
419 White arrow: granulocyte infiltration; Black arrow: inclusion bodies; Black star: hystiocytosis; White
420 arrowhead: syncytial cells; Black arrowhead: necrotic inclusion bodies. NS/NA represents samples were
421 immunopathogenic manifestations were not shown/not analyzed. Scale bar represents the size of analyzed
422 portions.

423

424 Regarding NiV-Ban IP infections, three out of four IFNAR KO animals were positive to NiV-N
425 protein immunolabeling (Fig. 5A, left panel). Two of them exerted a positive labeling for NiV
426 antigen in both lung and spleen, with a cellular tropism for pneumocytes and large mononuclear
427 cells of the spleen marginal zone, respectively (Fig. 5B). In the lung, the presence of the virus was
428 associated with perivascular inflammation and syncytial cells, which were diffused throughout
429 alveoli, vessels and bronchi (Fig. 6). In the spleen, syncytia and necrosis were observed mainly in
430 expanded marginal zones that were rich in mononuclear cells, which was indicative of histiocytosis
431 (Fig. 6). In the third IFNAR KO animal, diffused NiV-N staining was found in the brain (lungs
432 and spleens were not available) (Fig. 5A, left panel and 5B). Moreover, this animal displayed
433 extensive lesions corresponding to non-suppurative necrotizing encephalitis and meningitis with
434 perivascular cuffing (Fig. 6).

435 Regarding the analysis of IN-infected animals, since viral RNA was detected in few samples, we
436 selected animals that were positive for further immunohistochemistry analysis only (Fig. 5A, right
437 panel, 5B, 6, S2 and S3). Out of these 20 animals, only 5 resulted positive for NiV antigen labeling,
438 suggesting that RNA detection is more sensitive than protein labeling (Fig. 5A, right panel and
439 5B). In both murine genotypes, few cells positive for NiV antigen were detected, and the major
440 histological observation was the presence of perivascular inflammatory cell infiltration in lungs
441 and focal expansion of the marginal zone in spleen (Fig. 6 and S3). The WT mouse that succumbed
442 to NiV-Mal infection at d20 was positive for NiV Ag in the brain and displayed focal encephalitis
443 associated with histiocytosis (Fig. S3). No NiV antigen or histopathological lesions were detected
444 in the brain of other IN-infected animals.

445

446 Discussion

447 More than 25 years after its first isolation, NiV remains a global health threat due to its high
448 lethality, its human-to-human transmission and the lack of approved therapeutics. Both NiV-Mal
449 and NiV-Ban strains are associated with different symptoms and lethality (35). It is possible that
450 the CFR associated to outbreaks is influenced by multiple factors, such as the viral dose of
451 infection and the route of transmission, as well as socio-economic factors such as Public Health
452 measures and access to healthcare (8,36,37). Indeed, while NiV-Mal emerged only twice in 1998-
453 1999 and 2014, NiV-Ban re-emerged frequently since 2001 (38). Nonetheless, two bats in a city
454 market in Central Java, Indonesia, have been reported positive to NiV-Mal recently, highlighting
455 the risk of spillover from both viral strains (39). The causes responsible for the different diseases
456 associated to NiV-Mal- and NiV-Ban-infected patients remain unclear, and multiple animal

457 models have been tested to characterize its respective pathogenesis (25,28,29,40–47). While non-
458 human primates, hamsters and ferrets succumb to NiV infection, WT mice clear the virus despite
459 being permissive to viral replication (25). However, we previously demonstrated that IFNAR KO
460 mice die following NiV-Mal intraperitoneal challenge due to the lack of type I IFN signaling (25).
461 So far, experiments involving NiV-Ban infection in murine models are lacking and may be of
462 interest to evaluate pathogenic differences between both viral strains *in vivo*. Here, we compared
463 NiV-Mal and NiV-Ban challenge in both WT and IFNAR KO mice infected through the IP or IN
464 route of inoculation.

465 First, we demonstrated that WT and IFNAR KO primary MEFs are both permissive to NiV-Mal
466 and NiV-Ban infections. Our experiments determined notable differences in the kinetic and the
467 size of formed syncytia in both MEFs genotypes with IFNAR KO cells being more prone to viral
468 dissemination compared to WT cells, along NiV-Mal strain expanding faster than NiV-Ban, thus
469 confirming previous observations made in hamster model (40,42). Then, we investigated such
470 disparities *in vivo* by challenging WT and IFNAR KO mice with each NiV strain through the IP
471 or IN route. Indeed, consistent with our *in vitro* observations, higher lethality was observed in
472 IFNAR KO following NiV-Mal infection compared to NiV-Ban infection through the IP route,
473 while all WT mice survived. Surprisingly, all IFNAR KO mice including animals infected with
474 NiV-Ban, known to be associated with respiratory distress syndrome in humans, survived IN
475 infection. Indeed, contrary to the IP route, IN inoculation led to a subclinical infection with both
476 NiV strains in IFNAR KO mice, thus confirming previous observations where the IN route lead to
477 an attenuated disease (25). Also, the lower inoculation dose (10^5 PFU) used for IN challenge in
478 this study compared to the dose used in our previous report (10^6 PFU) might be responsible for the
479 absence of fatal outcomes (25). Overall, contrary to the human-associated NiV disease observed
480 in African green monkeys, rodents including our murine models may fail to recapitulate NiV
481 morbidities and outcomes (40,46), potentially due to species-specific factors, such as a more
482 developed basal immune environment in the respiratory tract when compared with primates (48–
483 50).

484

485 Concomitantly, IN-inoculated and surviving IP-inoculated IFNAR KO mice produced
486 significantly higher nAb titers compared to WT mice following NiV infection with both strains.
487 This demonstrates that despite the lack of IFN-I signaling-dependent activity and higher viral
488 replication, the adaptive immune response was strong enough to control viral growth. Interestingly,
489 the lack of visible pathogenic signs in both WT and IFNAR KO mice following IN infection may
490 be related to a major role of type III IFNs in the defense against pathogens in mucosal barriers
491 such as the respiratory tract, as previously described (51–53). Regarding brain infection, few
492 analyzed samples were positive following IN inoculation, suggesting differences in viral entry in
493 the central nervous system (CNS) through the olfactory bulb as described in hamsters (54).
494 Intriguingly, in the mouse model, the hematogenous route resulted in a higher propension of the
495 virus to reach the CNS, as observed in IP-infected mice. Globally, considering the absence of
496 clinical symptoms and scarce viral propagation, murine models do not appear to be very

susceptible to IN infection. However, further tests with a higher inoculation dose or with combined KOs could clarify differences between NiV-Mal and NiV-Ban *in vivo* following IN inoculation.

Interestingly, a different cell tropism was observed in the lungs between the two viral strains following IP infection. NiV-Mal-associated antigen was mainly detected in the bronchi and BALT, while NiV-Ban mostly infected alveolar pneumocytes. Moreover, syncytia in the lungs were centered on blood vessels with NiV-Mal but were diffused throughout lung parenchyma and bronchi with NiV-Ban. Further investigations are necessary to understand whether the observed cellular tropism and syncytia distribution are host-specific and whether they have consequences on viral shedding. Furthermore, virus-induced cell-to-cell fusion has been demonstrated to be associated with STING responses and may contribute to disrupt the blood-brain barrier following NiV infection as well, but syncytia formation has not always been thoroughly analyzed in animal experiments in the literature (27,55–57). Thus, systematic reporting of syncytia formation in future studies could contribute to shed light into differences between NiV strains.

Concerning the spleen, two IFNAR KO animals which succumbed to NiV-Ban IP infection displayed foci of NiV-N antigen positive large mononuclear cells, corresponding to macrophages, in the mantle zone. This demonstrates that despite antigen interaction/potential internalization by antigen-presenting-cells (APCs) in the spleen, the immune response was not fast and/or strong enough to control infection.

In the brain, no strain-specific differences in cell tropism were observed and viruses were found in diverse compartments, including meninges and olfactory bulb. This corroborates the observation that NiV can potentially distribute and induce lesions throughout the whole brain, as recently reported by Goldin *et al*. following NiV-Ban infection in AGMs (58). Moreover, while both viral strains could induce similar lesions in the brain, the capacity of NiV-Ban to reach the brain in humans is restrained due to the fast and severe respiratory syndrome it induces, thus limiting its ability to further affect the brain. This was supported by Goldin *et al.*, who reported that treatments counteracting NiV-Ban respiratory disease ultimately led to the death of monkeys through encephalitis (58).

Altogether, we tested IFNAR KO mice as potential experimental model for both NiV-Mal and NiV-Ban infections. IP infection resulted in lethal outcome in 100% of NiV-Mal- and 60% of NiV-Ban-infected mice in this model with viral replication detected in all tested organs. Conversely, IN inoculation induced a subclinical infection with both viral strains. While hamsters and AGMs are the most suitable models to study NiV infection due to their natural susceptibility to the virus, mice could represent a useful alternative due to the large number of immune reagents, genetic tools and global knowledge in murine immune system available. Interestingly, the NiV-Ban IP-infected IFNAR KO model is of high interest to study chronic NiV infection as NiV-positive animals without symptoms were identified after 32 days, thus representing a potential model to challenge therapeutics against cerebral infection. Moreover, the possibility to produce specific KO mice may allow further dissect the contribution of specific immune factors involved in the control of NiV. In conclusion, mice represent a valid small animal model for specific immunopathogenic and fundamental investigations in the study of NiV infection.

CRediT authorship contribution statement

Conceptualization: MI, BH; Acquisition and analysis of data: LA, BP, DD, IR, JSp, JSk, TL, OT; Writing Original Draft: LA, BH, OR, MI; Providing critical methodology: UK, JSp, JSk; Supervision: BH, MI; Funding Acquisition: BH, MI.

Acknowledgements

The study was supported by ERINHA-Advance (ICONIM) and by Aviesan Sino-French agreement on Nipah virus study and by INSERM. We are grateful to all the members of the group Immunobiology of viral infection at CIRI, and Audrey Richard and Claudia Filippone from ERINHA, for the help in the realization of this study. We thank Professor Yuke-Fun Chan of University of Malaya for kindly providing Nipah virus Malaysia strain. We thank to Center for Disease Control and Prevention, Atlanta, USA, for kindly providing Nipah virus Bangladesh isolate. We acknowledge the contribution of the SFR Biosciences (UMS3444/CNRS, US8/Inserm) in Lyon.

551 **Bibliography**

552 1. Pelissier R, Iampietro M, Horvat B. Recent advances in the understanding of Nipah virus
553 immunopathogenesis and anti-viral approaches. F1000Research. 2019 Oct 16;8:1763.

554 2. Enchéry F, Horvat B. Understanding the interaction between henipaviruses and their natural
555 host, fruit bats: Paving the way toward control of highly lethal infection in humans. Int Rev
556 Immunol. 2017 Mar 4;36(2):108–21.

557 3. Mougari S, Gonzalez C, Reynard O, Horvat B. Fruit bats as natural reservoir of highly
558 pathogenic henipaviruses: balance between antiviral defense and viral toleranceInteractions
559 between Henipaviruses and their natural host, fruit bats. Curr Opin Virol. 2022
560 June;54:101228.

561 4. Branda F, Ceccarelli G, Giovanetti M, Albanese M, Binetti E, Ciccozzi M, et al. Nipah
562 Virus: A Zoonotic Threat Re-Emerging in the Wake of Global Public Health Challenges.
563 Microorganisms. 2025 Jan 9;13(1):124.

564 5. Epstein JH, Anthony SJ, Islam A, Kilpatrick AM, Ali Khan S, Balkey MD, et al. Nipah virus
565 dynamics in bats and implications for spillover to humans. Proc Natl Acad Sci. 2020 Nov
566 17;117(46):29190–201.

567 6. Letko M, Seifert SN, Olival KJ, Plowright RK, Munster VJ. Bat-borne virus diversity,
568 spillover and emergence. Nat Rev Microbiol. 2020 Aug;18(8):461–71.

569 7. Pulliam JRC, Epstein JH, Dushoff J, Rahman SA, Bunning M, Jamaluddin AA, et al.
570 Agricultural intensification, priming for persistence and the emergence of Nipah virus: a
571 lethal bat-borne zoonosis. J R Soc Interface. 2012 Jan 7;9(66):89–101.

572 8. Bruno L, Nappo MA, Ferrari L, Di Lecce R, Guarnieri C, Cantoni AM, et al. Nipah Virus
573 Disease: Epidemiological, Clinical, Diagnostic and Legislative Aspects of This
574 Unpredictable Emerging Zoonosis. Animals. 2022 Dec 31;13(1):159.

575 9. Eby P, Peel AJ, Hoegh A, Madden W, Giles JR, Hudson PJ, et al. Pathogen spillover driven
576 by rapid changes in bat ecology. Nature. 2023 Jan;613(7943):340–4.

577 10. Harcourt BH, Lowe L, Tamin A, Liu X, Bankamp B, Bowden N, et al. Genetic
578 characterization of Nipah virus, Bangladesh, 2004. Emerg Infect Dis. 2005 Oct;11(10):1594–
579 7.

580 11. Wong KT, Shieh WJ, Kumar S, Norain K, Abdullah W, Guarner J, et al. Nipah Virus
581 Infection: Pathology and Pathogenesis of an Emerging Paramyxoviral Zoonosis. Am J
582 Pathol. 2002 Dec 1;161(6):2153–67.

583 12. Satter SM, Aquib WR, Sultana S, Sharif AR, Nazneen A, Alam MR, et al. Tackling a global
584 epidemic threat: Nipah surveillance in Bangladesh, 2006-2021. PLoS Negl Trop Dis. 2023
585 Sept;17(9):e0011617.

586 13. Islam MS, Sazzad HMS, Satter SM, Sultana S, Hossain MJ, Hasan M, et al. Nipah Virus
587 Transmission from Bats to Humans Associated with Drinking Traditional Liquor Made from
588 Date Palm Sap, Bangladesh, 2011-2014. Emerg Infect Dis. 2016 Apr;22(4):664–70.

589 14. Johnson C, Dee M. Nipah virus: Awareness for anesthesia providers and perioperative
590 management strategies. JCA Adv. 2025 Sept;2(3):100140.

591 15. Hsu VP, Hossain MJ, Parashar UD, Ali MM, Ksiazek TG, Kuzmin I, et al. Nipah virus
592 encephalitis reemergence, Bangladesh. Emerg Infect Dis. 2004 Dec;10(12):2082–7.

593 16. Nazmunnahar null, Ahmed I, Roknuzzaman ASM, Islam MR. The recent Nipah virus
594 outbreak in Bangladesh could be a threat for global public health: A brief report. Health Sci
595 Rep. 2023 July;6(7):e1423.

596 17. Luby SP, Hossain MJ, Gurley ES, Ahmed BN, Banu S, Khan SU, et al. Recurrent zoonotic
597 transmission of Nipah virus into humans, Bangladesh, 2001-2007. Emerg Infect Dis. 2009
598 Aug;15(8):1229–35.

599 18. Negrete OA, Levroney EL, Aguilar HC, Bertolotti-Ciarlet A, Nazarian R, Tajyar S, et al.
600 EphrinB2 is the entry receptor for Nipah virus, an emergent deadly paramyxovirus. Nature.
601 2005 July 21;436(7049):401–5.

602 19. Bonaparte MI, Dimitrov AS, Bossart KN, Crameri G, Mungall BA, Bishop KA, et al.
603 Ephrin-B2 ligand is a functional receptor for Hendra virus and Nipah virus. Proc Natl Acad
604 Sci U S A. 2005;102(30):10652–7.

605 20. Negrete OA, Wolf MC, Aguilar HC, Enterlein S, Wang W, M√ºhlberger E, et al. Two key
606 residues in ephrinB3 are critical for its use as an alternative receptor for Nipah virus. PLoS
607 Pathog. 2006;2(2):e7–e7.

608 21. Dhondt KP, Horvat B. Henipavirus Infections: Lessons from Animal Models. Pathogens.
609 2013 Apr 9;2(2):264–87.

610 22. Rockx B. Recent developments in experimental animal models of Henipavirus infection.
611 Pathog Dis. 2014 July;71(2):199–206.

612 23. Iampietro M, Aurine N, Dhondt KP, Dumont C, Pelissier R, Spanier J, et al. Control of
613 Nipah Virus Infection in Mice by the Host Adaptors Mitochondrial Antiviral Signaling
614 Protein (MAVS) and Myeloid Differentiation Primary Response 88 (MyD88). J Infect Dis.
615 2020 May 11;221(Supplement_4):S401–6.

616 24. Davies KA, Welch SR, Coleman-McCray JD, Sorvillo TE, Aida-Ficken V, Spiropoulou CF,
617 et al. Natural History of Nipah Virus in Hamsters: Strain, Route, and Sex-Associated
618 Variability Characterized using Large Datasets to Inform Pre-Clinical Study Design. J Infect
619 Dis. 2025 Oct 29;jiaf549.

620 25. Dhondt KP, Mathieu C, Chalons M, Reynaud JM, Vallve A, Raoul H, et al. Type I interferon
621 signaling protects mice from lethal henipavirus infection. J Infect Dis. 2013 Jan
622 1;207(1):142–51.

623 26. Iampietro M, Dumont C, Mathieu C, Spanier J, Robert J, Charpenay A, et al. Activation of
624 cGAS/STING pathway upon paramyxovirus infection. iScience. 2021 June 25;24(6):102519.

625 27. Amurri L, Dumont C, Pelissier R, Reynard O, Mathieu C, Spanier J, et al. Multifaceted
626 activation of STING axis upon Nipah and measles virus-induced syncytia formation. Kuhn
627 JH, editor. PLOS Pathog. 2024 Sept 16;20(9):e1012569.

628 28. Dups J, Middleton D, Long F, Arkinstall R, Marsh GA, Wang LF. Subclinical infection
629 without encephalitis in mice following intranasal exposure to Nipah virus-Malaysia and
630 Nipah virus-Bangladesh. Virol J. 2014;11.

631 29. Edwards SJ, Rowe B, Reid T, Tachedjian M, Caruso S, Blasdell K, et al. Henipavirus-
632 induced neuropathogenesis in mice. Virology. 2023 Oct;587:109856.

633 30. Muller U, Steinhoff U, Reis LF, Hemmi S, Pavlovic J, Zinkernagel RM, et al. Functional
634 role of type I and type II interferons in antiviral defense. Science. 1994 June
635 24;264(5167):1918–21.

636 31. Brune W, Hengel H, Koszinowski UH. A mouse model for cytomegalovirus infection. Curr
637 Protoc Immunol. 2001 Aug;Chapter 19:Unit 19.7.

638 32. Hennings TG, Chopra DG, DeLeon ER, VanDeusen HR, Sesaki H, Merrins MJ, et al. In
639 Vivo Deletion of β-Cell Drp1 Impairs Insulin Secretion Without Affecting Islet Oxygen
640 Consumption. Endocrinology. 2018 Sept 1;159(9):3245–56.

641 33. Pfaffl MW. A new mathematical model for relative quantification in real-time RT-PCR.
642 Nucleic Acids Res. 2001 May 1;29(9):e45.

643 34. Bustin SA, Benes V, Garson JA, Hellemans J, Huggett J, Kubista M, et al. The MIQE
644 Guidelines: Minimum Information for Publication of Quantitative Real-Time PCR
645 Experiments. Clin Chem. 2009 Apr 1;55(4):611–22.

646 35. Wang L, Lu D, Yang M, Chai S, Du H, Jiang H. Nipah virus: epidemiology, pathogenesis,
647 treatment, and prevention. Front Med. 2024 Dec;18(6):969–87.

648 36. Johnson T, Jamrozik E, Hurst T, Cheah PY, Parker MJ. Ethical issues in Nipah virus control
649 and research: addressing a neglected disease. J Med Ethics. 2024 Aug 21;50(9):612–7.

650 37. Suit-B Y, Hassan L, Krauss SE, Ooi PT, Ramanoon SZ, Yasmin AR, et al. Mental Model of
651 Malaysian Pig Farmers in Implementing Disease Prevention and Control Practices. Front Vet
652 Sci. 2021;8:695702.

653 38. Bhowmik A, Hasan M, Redoy MMH, Saha G. Nipah virus outbreak trends in Bangladesh
654 during the period 2001 to 2024: a brief review. Sci One Health. 2025;4:100103.

655 39. Putro DBW, Mulyono A, Rahardianingtyas E, Ardanto A, Joharina AS, Hidajat MC, et al.
656 Nipah Virus Detection in Pteropus hypomelanus Bats, Central Java, Indonesia. Emerg Infect
657 Dis. 2025 Apr;31(4):867–70.

658 40. DeBuysscher BL, de Wit E, Munster VJ, Scott D, Feldmann H, Prescott J. Comparison of
659 the pathogenicity of Nipah virus isolates from Bangladesh and Malaysia in the Syrian
660 hamster. PLoS Negl Trop Dis. 2013;7(1).

661 41. Baseler L, de Wit E, Scott DP, Munster VJ, Feldmann H. Syrian hamsters (Mesocricetus
662 auratus) oronasally inoculated with a Nipah virus isolate from Bangladesh or Malaysia
663 develop similar respiratory tract lesions. Vet Pathol. 2015 Jan;52(1):38–45.

664 42. Baseler L, Scott DP, Saturday G, Horne E, Rosenke R, Thomas T, et al. Identifying Early
665 Target Cells of Nipah Virus Infection in Syrian Hamsters. Geisbert T, editor. PLoS Negl
666 Trop Dis. 2016 Nov;10(11):e0005120–e0005120.

667 43. Griffin BD, Leung A, Chan M, Warner BM, Ranadheera C, Tierney K, et al. Establishment
668 of an RNA polymerase II-driven reverse genetics system for Nipah virus strains from
669 Malaysia and Bangladesh. Sci Rep. 2019 Aug 1;9(1):11171.

670 44. Clayton BA, Middleton D, Bergfeld J, Haining J, Arkinstall R, Wang L, et al. Transmission
671 routes for nipah virus from Malaysia and Bangladesh. Emerg Infect Dis. 2012
672 Dec;18(12):1983–93.

673 45. Clayton BA, Middleton D, Arkinstall R, Frazer L, Wang LF, Marsh GA. The Nature of
674 Exposure Drives Transmission of Nipah Viruses from Malaysia and Bangladesh in Ferrets.
675 PLoS Negl Trop Dis. 2016 June 24;10(6):e0004775.

676 46. Leon AJ, Borisevich V, Boroumand N, Seymour R, Nusbaum R, Escaffre O, et al. Host gene
677 expression profiles in ferrets infected with genetically distinct henipavirus strains. PLoS
678 Negl Trop Dis [Internet]. 2018 Mar 14 [cited 2019 June 24];12(3). Available from:
679 https://www.ncbi.nlm.nih.gov/pmc/articles/PMC5868854/

680 47. Mire CE, Satterfield BA, Geisbert JB, Agans KN, Borisevich V, Yan L, et al. Pathogenic
681 Differences between Nipah Virus Bangladesh and Malaysia Strains in Primates: Implications
682 for Antibody Therapy. Sci Rep. 2016 Aug 3;6:30916.

683 48. Mestas J, Hughes CCW. Of mice and not men: differences between mouse and human
684 immunology. J Immunol Baltim Md 1950. 2004 Mar 1;172(5):2731–8.

685 49. Pabst R, Gehrke I. Is the bronchus-associated lymphoid tissue (BALT) an integral structure
686 of the lung in normal mammals, including humans? Am J Respir Cell Mol Biol. 1990
687 Aug;3(2):131–5.

688 50. Bjornson-Hooper ZB, Fragiadakis GK, Spitzer MH, Chen H, Madhireddy D, Hu K, et al. A
689 Comprehensive Atlas of Immunological Differences Between Humans, Mice, and Non-
690 Human Primates. Front Immunol. 2022;13:867015.

691 51. Wells AI, Coyne CB. Type III Interferons in Antiviral Defenses at Barrier Surfaces. Trends
692 Immunol. 2018 Oct;39(10):848–58.

693 52. Lazear HM, Schoggins JW, Diamond MS. Shared and Distinct Functions of Type I and Type
694 III Interferons. Immunity. 2019 Apr 16;50(4):907–23.

695 53. Stanifer ML, Guo C, Doldan P, Boulant S. Importance of Type I and III Interferons at
696 Respiratory and Intestinal Barrier Surfaces. Front Immunol. 2020;11:608645.

697 54. Munster VJ, Prescott JB, Bushmaker T, Long D, Rosenke R, Thomas T, et al. Rapid Nipah
698 virus entry into the central nervous system of hamsters via the olfactory route. Sci Rep.
699 2012;2:736.

700 55. Gamble A, Yeo YY, Butler AA, Tang H, Snedden CE, Mason CT, et al. Drivers and
701 Distribution of Henipavirus-Induced Syncytia: What Do We Know? Viruses. 2021 Sept
702 2;13(9):1755.

703 56. Weingartl H, Czub S, Copps J, Berhane Y, Middleton D, Marszal P, et al. Invasion of the
704 central nervous system in a porcine host by nipah virus. J Virol. 2005 June;79(12):7528–34.

705 57. Rockx B, Brining D, Kramer J, Callison J, Ebihara H, Mansfield K, et al. Clinical Outcome
706 of Henipavirus Infection in Hamsters is Determined by the Route and Dose of Infection. J
707 Virol. 2011 May 18;85(11):7658–71.

708 58. Goldin K, Liu Y, Rosenke R, Prado-Smith J, Flagg M, de Wit E. Nipah Virus-Associated
709 Neuropathology in African Green Monkeys During Acute Disease and Convalescence. J
710 Infect Dis. 2025 Feb 4;231(1):219–29.

712 ## Supporting information

713

714 **S1 Fig. Different pathogenic signatures of NiV Mal and NiV-Ban infection in mice *in vivo*.**
715 WT and IFNAR KO mice were infected through an intraperitoneal route (A, C) or intranasal route
716 (B, D) with 10^6 or 10^5 PFU, respectively, of NiV-Mal or NiV-Ban. All groups were constituted of
717 5 animals except for NiV-Mal IFNAR KO group, which consisted of 6 mice. Animals were
718 monitored for 32 days for weight (A-B) and clinical signs with established clinical scores (C-D).

719

720 **S2 Fig. NiV infection is attenuated in WT mice.** Organs from selected animals were included in
721 paraffin and sections were stained with a rabbit polyclonal anti-NiV-N antibody and DAPI for
722 immunohistochemistry analysis. (A) Brain, lung and spleens sections from WT mice were used as
723 NiV-negative control conditions while similar sections from WT mice sensitive to NiV infection
724 were used to characterize the presence of NiV-N antigens. NS/NA represents samples were NiV-
725 N was not shown/not analyzed. Scale bar represents the size of analyzed portions.

726

727 **S3 Fig. Intraperitoneal and intranasal NiV infections generate mild immunopathogenesis in**
728 **WT mice.** Organs from selected animals underwent hematoxylin-eosin-saffron (HES) staining and
729 were evaluated by a board-certified veterinary pathologist. Brain, lung and spleens sections from
730 WT mice were used as control conditions while similar sections from WT mice sensitive to NiV
731 infection were used to characterize the presence of immunopathogenic manifestations. Black star:
732 hystiocytosis; White arrowhead: syncytial cells. NS/NA represents samples were
733 immunopathogenic manifestations were not shown/not analyzed. Scale bar represents the size of
734 analyzed portions.

Fig. 1

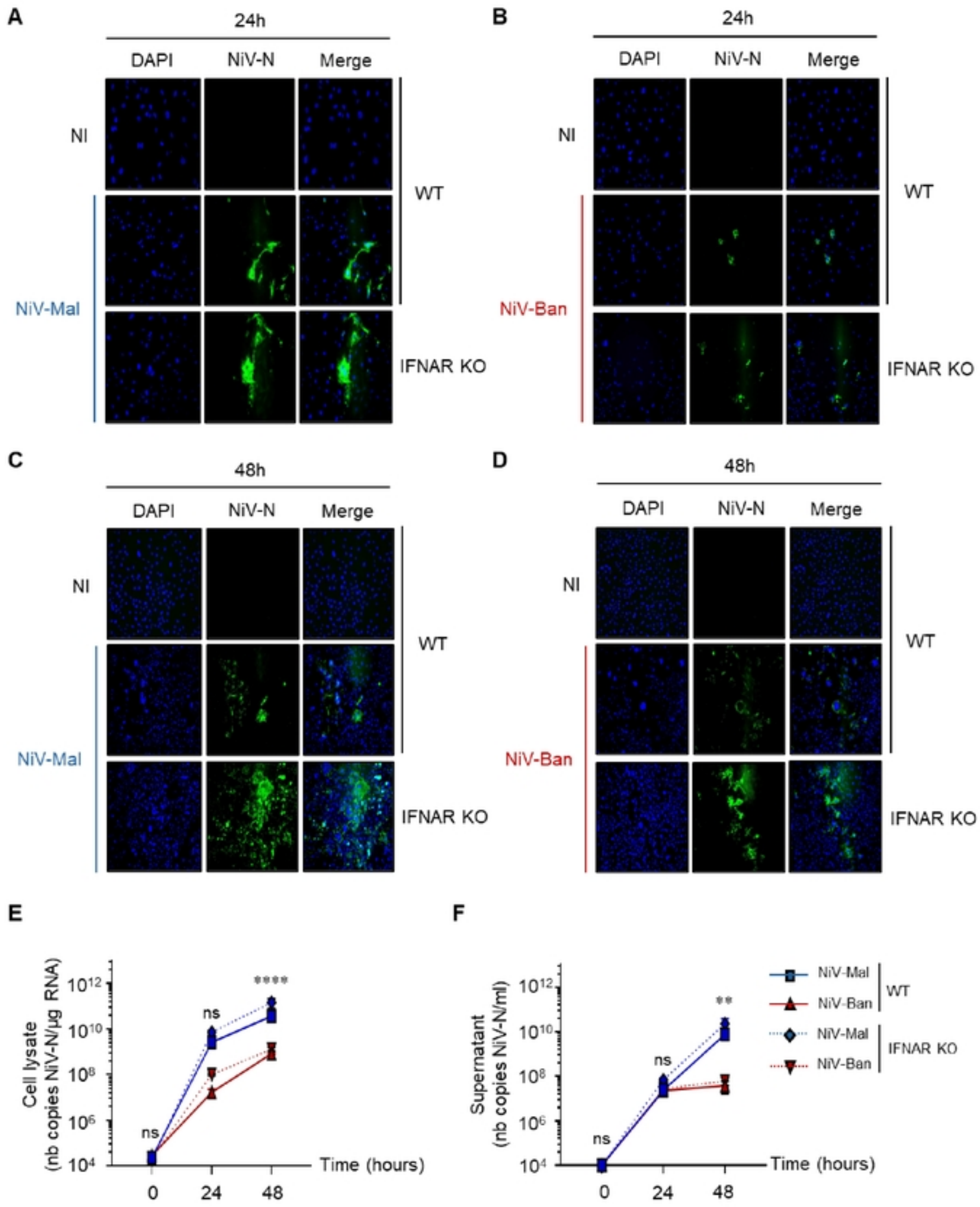
A
24h
DAPI
NiV-N
Merge
NI
WT
NiV-Mal
IFNAR KO
B
24h
DAPI
NiV-N
Merge
NI
WT
NiV-Ban
IFNAR KO
C
48h
DAPI
NiV-N
Merge
NI
WT
NiV-Mal
IFNAR KO
D
48h
DAPI
NiV-N
Merge
NI
WT
NiV-Ban
IFNAR KO
E
Cell lysate
(nb copies NiV-N/µg RNA)
10^{12}
10^{10}
10^{8}
10^{6}
10^{4}
ns
ns
****
Time (hours)
0
24
48
F
Supernatant
(nb copies NiV-N/ml)
10^{12}
10^{10}
10^{8}
10^{6}
10^{4}
ns
ns
**
Time (hours)
0
24
48
NiV-Mal
NiV-Ban
WT
NiV-Mal
NiV-Ban
IFNAR KO

Fig. 2

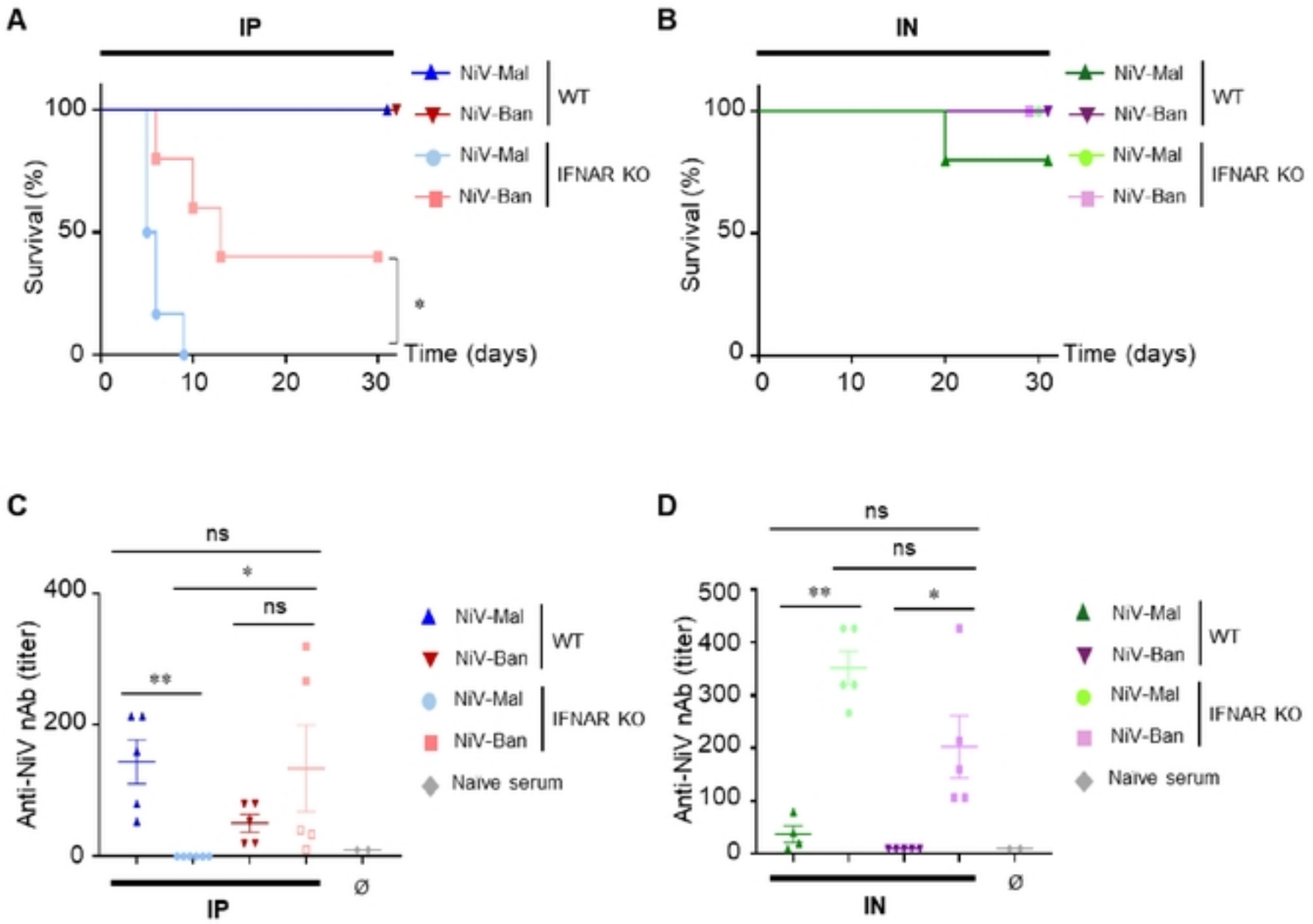
A
IP
Survival (%)
100
50
0
0
10
20
30
Time (days)
*
NiV-Mal
NiV-Ban
WT
NiV-Mal
NiV-Ban
IFNAR KO
B
IN
Survival (%)
100
50
0
0
10
20
30
Time (days)
NiV-Mal
NiV-Ban
WT
NiV-Mal
NiV-Ban
IFNAR KO
C
ns
*
ns
**
Anti-NiV nAb (titer)
400
200
0
NiV-Mal
NiV-Ban
WT
NiV-Mal
NiV-Ban
IFNAR KO
Naive serum
Ø
IP
D
ns
ns
**
*
Anti-NiV nAb (titer)
500
400
300
200
100
0
NiV-Mal
NiV-Ban
WT
NiV-Mal
NiV-Ban
IFNAR KO
Naive serum
Ø
IN

Fig. 3

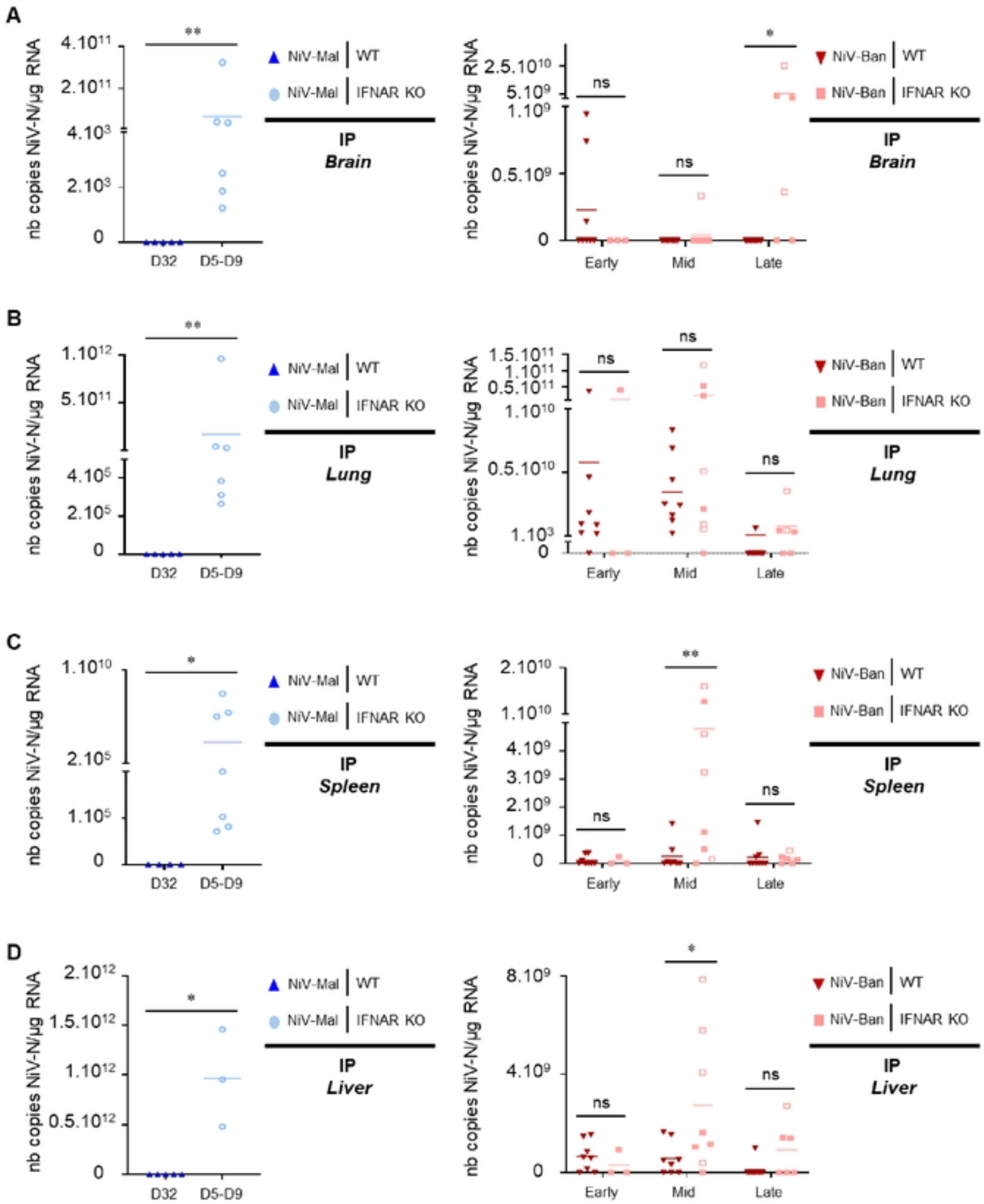
A
B
C
D
nb copies NiV-N/µg RNA
NiV-Mal | WT
NiV-Mal | IFNAR KO
NiV-Ban | WT
NiV-Ban | IFNAR KO
IP
Brain
Lung
Spleen
Liver
D32
D5-D9
Early
Mid
Late
ns
*
**

Fig. 4

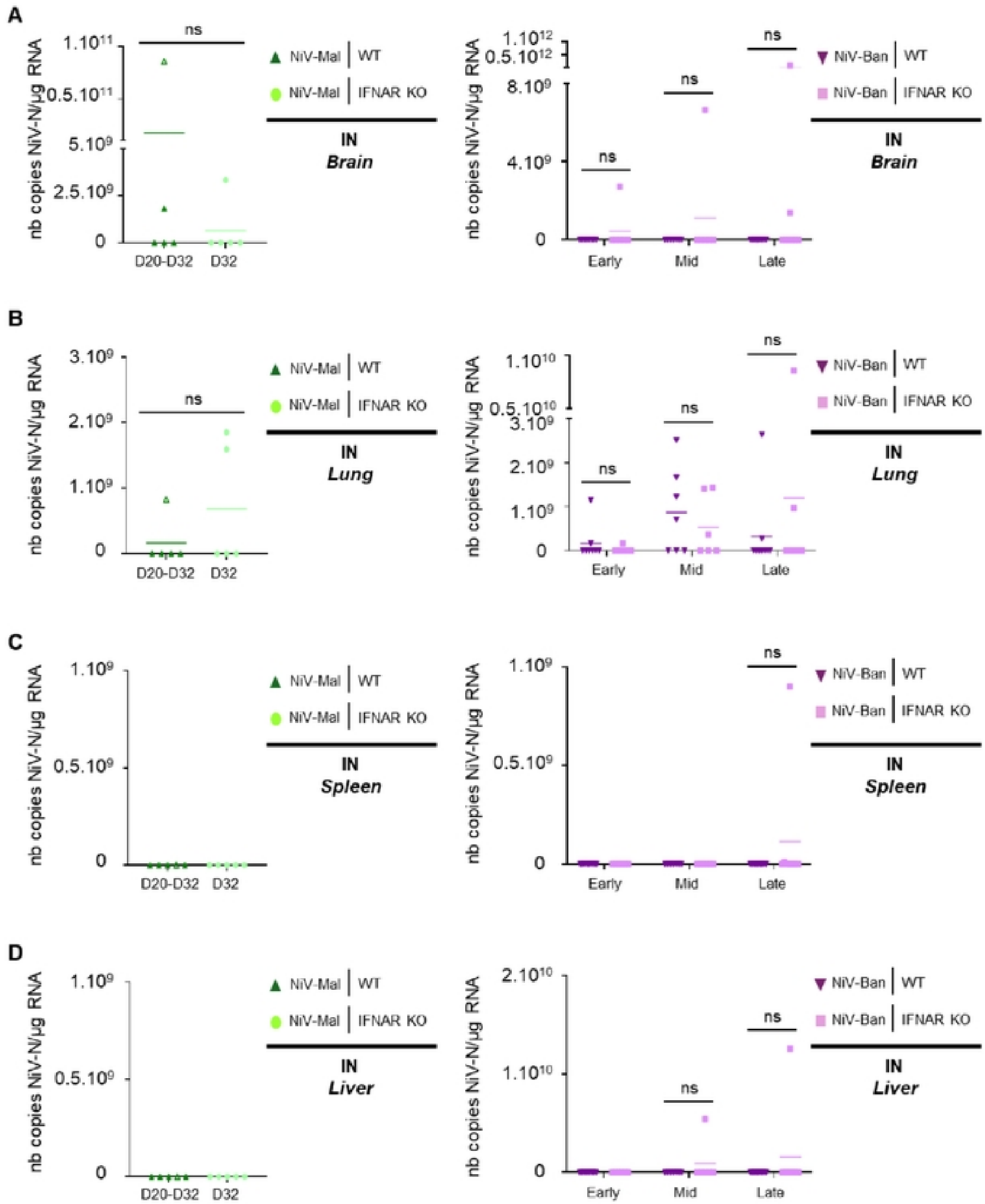
A
B
C
D
nb copies NiV-N/µg RNA
ns
NiV-Mal | WT
NiV-Mal | IFNAR KO
NiV-Ban | WT
NiV-Ban | IFNAR KO
IN
Brain
Lung
Spleen
Liver
D20-D32
D32
Early
Mid
Late

Fig. 5

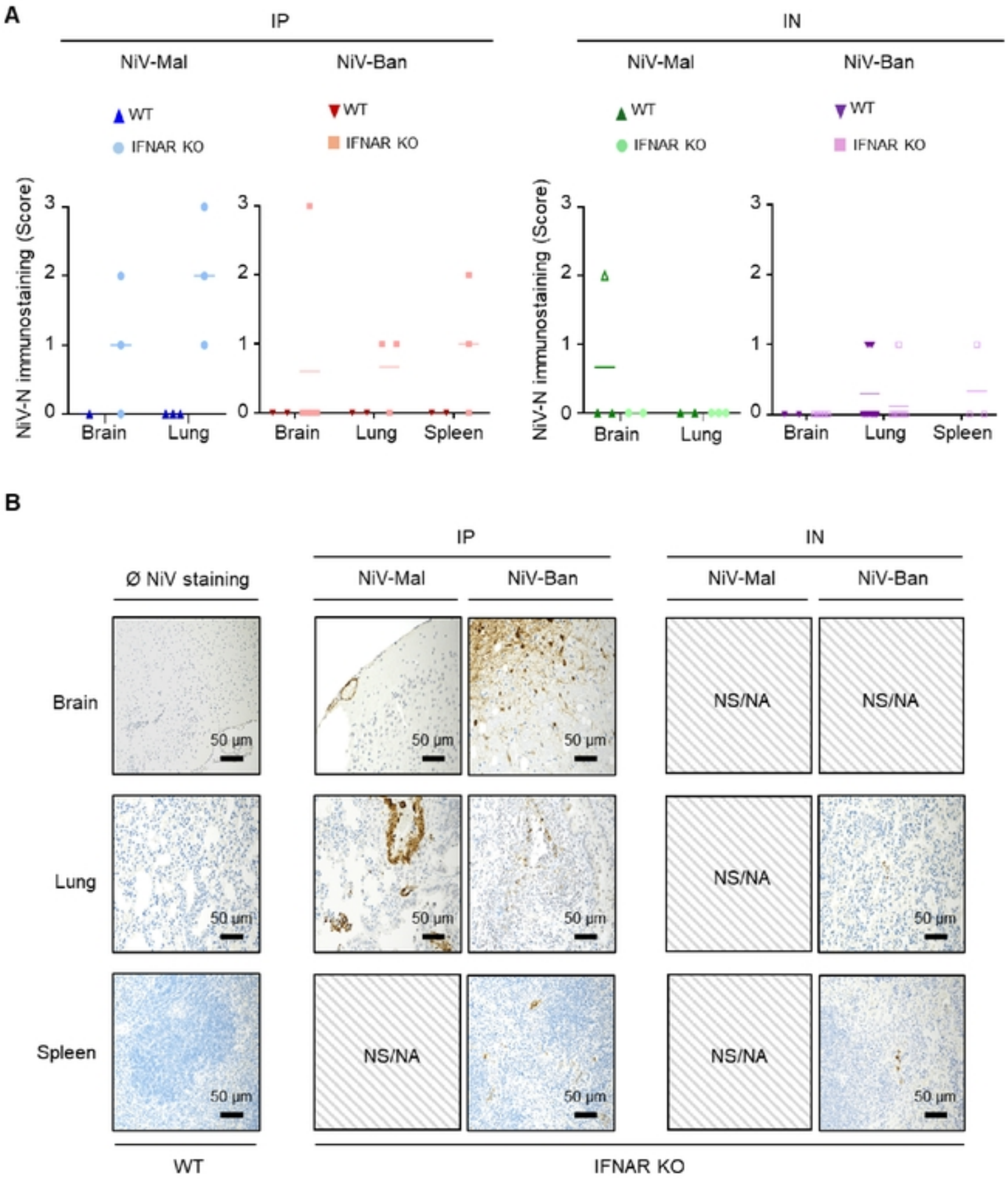
A
IP
IN
NiV-Mal
NiV-Ban
WT
IFNAR KO
NiV-N immunostaining (Score)
Brain
Lung
Spleen
B
Ø NiV staining
NS/NA
50 µm
WT
IFNAR KO

Fig. 6

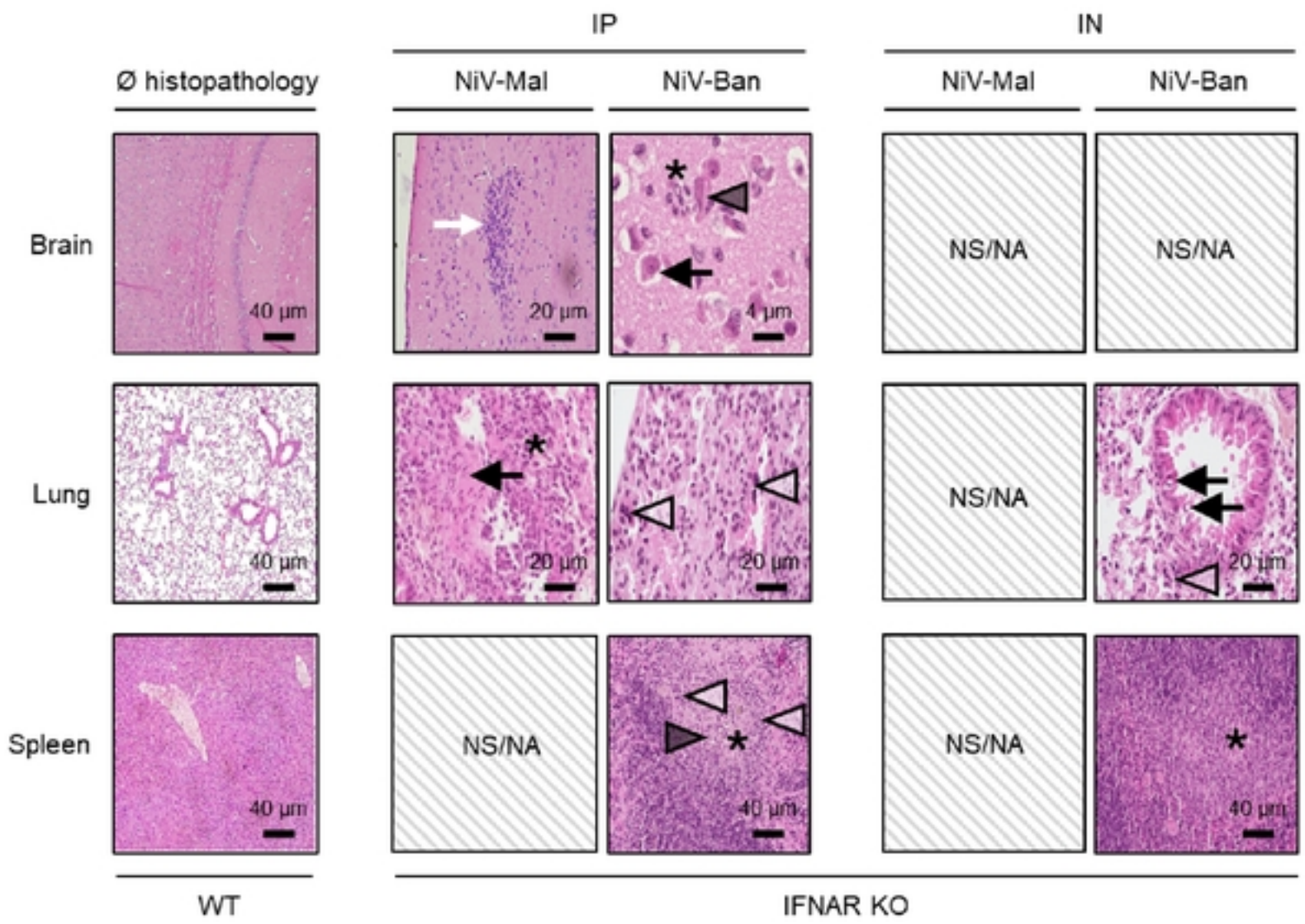
IP
IN
Ø histopathology
NiV-Mal
NiV-Ban
NiV-Mal
NiV-Ban
Brain
Lung
Spleen
NS/NA
40 µm
20 µm
4 µm
WT
IFNAR KO